Remarks

The following remarks are provided in further support of the Claims.

Present Status of the Claims: Claims 1-14 are pending.

Objections:

The figures are objected to as not showing the intended invention.

Rejections:

Rejection Under 35 U.S.C. §112

Claims 1-14 are rejected under 35 U.S. C. §112 second paragraph as being indefinite, vague, and confusing for failing to particularly point out and distinctly claim the subject matter which the applicant regards as the invention.

Rejection Under 35 U.S.C. §102(a)

Claims 1-4, 8, 9, 11, and 12 are rejected under 35 U.S.C. §102(a) as being unpatentable over Nunoue et al.

Claims 1, 3, 4, 8, and 12 are rejected under 35 U.S.C. §102(a) as being unpatentable over Koide et al.

Claims 1, 3, 4, and 8 are rejected under 35 U.S.C. §102(a) as being unpatentable over Khare et al.

Rejection Under 35 U.S.C. §103(a)

Claims 5-7, 10, 13, and 14 are rejected under 35 U.S.C. §103(a) as being unpatentable over Nunoue et al.

I. DISCUSSION - OBJECTIONS

The Office asserts that "the figures are objected because it does not show the intended invention." Fig. 2a includes a substrate, a nucleation layer, an interlayer, and multiple pairs of layers that form a supported distributed Bragg reflector, as in Claim 1.

PAGE 7/27 * RCVD AT 2/6/2004 10:55:25 AM [Eastern Standard Time] * SVR:USPTO-EFXRF-1/1 * DNIS:8729306 * CSID: * DURATION (mm-ss):08-44

Fig. 4a includes a substrate, a nucleation layer, a first interlayer, multiple pairs of layers, a second interlayer, and multiple pairs of layers that form a supported distributed Bragg reflector, as in Claim 13. The labels in the figures have been improved to make the identity of the layers clearer.

II. DISCUSSION - 35 U.S.C. §112

The Office rejected claims **1-14** under 35 U.S.C. §112, second paragraph, as being indefinite for failing to particularly point out and distinctly claim the subject matter which applicant regards as the Invention.

With respect to claim **1, 13, and 14** that the Office asserts to recite "a supported distributed Bragg reflector comprising: a substrate; a *nucleation layer* on substrate; an interlayer on nucleation layer, comprising a material selected from AlN, $Al_xGa_{1-x}N$ and AlBN and *multiple pairs of (Al,Ga,B)N/Al,Ga,B)N layers* on said interlayer forming a distributed Bragg reflector", the Office asserts that they are "vague and indefinite as to the make up of the nucleation layer, and confusing as to what pairs of material it is claiming-a mixture of ALL of the elements (Al,Ga,B)N, or a ONE mix-match of the element (AlGa,B)N pairs in the interlayer; if it is a mixture of ALL of the element AlN, AlGaN, and AlBN as multiple pairs interlayers." We address these points in the following paragraphs.

With respect to claims **1 and 14**, the Office asserts that the claims are indefinite as to the make up of the nucleation layer. The specific composition of the nucleation layer is dependent upon the substrate that is employed, as is known to those skilled in the art of III-V nitride material growth. We have amended the claims to define the required thickness in terms of its needed function of promoting continuous growth, which depends on the substrate.

With respect to claim **13**, the claim recites "a GaN nucleation layer having a thickness greater than approximately 0.5 microns," which does particularly point out and distinctly claim the makeup of the nucleation layer.

With respect to claims **1, 13, and 14**, the Office asserts that the claims are confusing as to what pairs of material it is claiming. The notation, (Al,Ga,B)N, is a standard general nomenclature used by those skilled in the art for group III-nitride

PAGE 8/27 * RCVD AT 2/6/2004 10:55:25 AM [Eastern Standard Time] * SVR:USPTO-EFXRF-1/1 * DNIS:8729306 * CSID: * DURATION (mm-ss):08-44

materials with different mole fractions of Al, Ga, and B with the individual elemental mole fractions ranging between 0 and 1. Additionally; the meaning is defined in the body of the specification on page 3 lines 26-30: "The (Al,Ga,B)N/(Al,Ga,B)N layered structure is commonly a AlGaN/GaN structure but can be more generally any Group III material-based structure such as AlBN, GaBN, AlGaN, or AlGaBN material paired with an AlN, GaN, or BN material. Indium can also be substituted. For the present invention, (Al,Ga,B)N/(Al,Ga,B)N represents any of the potential Group III material combinations that can be used." Solely for the purpose of clarification we have amended this nomenclature in claims **1,2,7,9, and 14** to be of the form $Al_wGa_xB_{1-w-x}N/Al_{w'}Ga_{x'}B_{1-w'-x'}N$. The particular group-III material compositions selected as pairs are determined by the wavelength of light that is to be reflected by the DBR; the criteria for selection of the proper combination are standard in the art and described in the references below. The structure and composition requirements are described in numerous regular and review articles on DBRs; for example, "Principles of Distributed Feedback and Distributed Bragg-Reflector Lasers", Shyh Wang, IEEE J. Quantum Electronics vol. QE10 #4 (1974) p. 413-427, "Effect of layer thickness variations in a distributed-Bragg reflector mirror on the phase of the reflected light," J.-P. Weber and Shyh Wang, Optics Lett. Vol. 15, No. 10 (1990) p. 526-528 and "Distributed Bragg Reflectors for Vertical-Cavity Surface-Emitting Lasers," by W.G. Breiland, A.A. Allerman, J.F. Klem, and K.E. Waldrip, MRS Bulletin Vol. 7 #7 (2002) p. 520-524. These are appended in whole or in part (first page only of Shyh Wang, 1974) to this submission.

With respect to claim **13** which recites "at least five pairs of $Al_yGa_{1-y}N$/GaN layers," the Office asserts that "it is not clear *the order structure* of these pairs layers." The necessary order structure of the pair layers to make a reflector is standard in the art and described in the references above.

With respect to claim **14** that recites a supported semiconductor lattice structure, the Office asserts that the claim is indefinite as to the differences of "*an interlayer* (Al,Ga,B)N and *a layer* of (Al,Ga,B)N." On page 2 of the specification, an "interlayer" is distinguished from a "layer" as comprising AlN or AlGaN interlayers that effectively control mismatch-induced stress and suppress the formation of cracks.

PAGE 9/27 * RCVD AT 2/6/2004 10:55:25 AM [Eastern Standard Time] * SVR:USPTO-EFXRF-1/1 * DNIS:8729306 * CSID: * DURATION (mm-ss):08-44

With respect to claims **6, 7, 14** that recite "greater than approximately," the Office asserts that "greater than *approximately*" is not a positive limitation. The limiting factor on how precisely the thickness of a semiconductor layer can be described is the thickness of one layer of Ga+N, Al+N, or Al+Ga+N atoms in the semiconductor crystal lattice. These layer thicknesses are determined by the lattice constants for the materials. Persons of ordinary skill in the art of growing epitaxial semiconductor structures can under optimized growth conditions control total layer thickness to one atomic layer thickness on each interface. The thickness of one layer is known for the a-direction and c-direction in wurtzite Group III-N semiconductors.

Lattice constants (Angstroms)	a-direction	c-direction
GaN	3.189	5.185
AlN	3.11	4.98
InN	3.54	5.70

From M.S. Shur and M.A. Khan, MRS Bull. 22 (2) 44 (1997)

For example, for growth on the c-face of a wurtzite crystal of GaN, AlN, or AlGaN, 20 Angstroms represents 4 monolayers of GaN, AlN, or AlGaN. With a possible variation in layer thickness of ± a few monolayers (± 5 Angstroms per monolayer), the typical variation in thickness across a device structure is an appreciable fraction of a total layer thickness of 20 Angstroms, so use of the term "approximately" is consistent with the precision possible in growing such structures. Persons of ordinary skill in the art of growing epitaxial semiconductor structures will understand this as a clear and enabling description of the structure of this invention.

With respect to claims **1, 13, and 14**, the Office asserts that there is insufficient structural and functional relationship to conform a distributed Bragg reflector, which renders the claims vague and indefinite. With respect to claims **1 and 13**, as discussed above, the necessary composition, thickness, and structure of the pair layers that comprise a distributed Bragg reflector are standard in the art and described in the references above. The particularities of a DBR structure are determined primarily by the

PAGE 10/27 * RCVD AT 2/6/2004 10:55:25 AM [Eastern Standard Time] * SVR:USPTO-EFXRF-1/1 * DNIS:8729306 * CSID: * DURATION (mm-ss):08-44

wavelength of its intended operation and requisite structure is well understood in accordance with prior art. Determination of the details of the incorporation of at least one stress-reducing interlayer in a DBR structure per this invention is within the scope of a person of ordinary skill in the art of growing DBR structures. With respect to claim **14**, the claim recites the formation of a supported semiconductor lattice structure that need not be a DBR so the specification of structural and functional relationships to conform a DBR is not required for the claim to be definite.

As the Office observes, claim **4** is dependent upon claim **1**, with the phrase "of claim **1**" having been omitted as a typographical error. Claim **4** properly reads "The supported distributed Bragg reflector of claim 1 wherein said nucleation layer comprises a GaN material." We have amended the claim.

As the Office observes, the phrase in claim **14**, "an interlayer comprising a material *selected form an* ..." contains a typographical error and should correctly read "an interlayer comprising a material *selected from an*..." We have amended the claim.

With respect to claims **2-12**, the Office rejects the claims on the same reason as claims **1, 13, and 14**. The responses above directed to the rejections of the latter claims are applicable to claims 2-12 as well.

III. DISCUSSION - 35 U.S.C. §102(a) Nunoue et al.

The Office rejected independent claim **1** and dependent claims **2-4, 8, 9, 11, and 12** under 35 U.S.C. §102(a) as being unpatentable over Nunoue et al. (US 20020036295)(2000-289396). Loss of right to patent under §102(a) requires that the invention be known or used by others in this country or be patented or described in a printed publication before the invention by the applicant. Nunoue et al. describes a DBR including a plurality of semiconductor layers made of a nitride semiconductor and a plurality of organic layers alternately laminated. It does not teach the suppression of cracking by the inclusion of stress-relieving interlayers to enable a high-reflectivity DBR as in our invention. It does not, therefore, show that the invention was known by others before our invention as claimed in independent claim 1 and dependent claims 2-4, 8, 9, 11, and 12.

PAGE 11/27 * RCVD AT 2/6/2004 10:55:25 AM [Eastern Standard Time] * SVR:USPTO-EFXRF-1/1 * DNIS:8729306 * CSID: * DURATION (mm-ss):08-44

IV. DISCUSSION - 35 U.S.C. §102(a) Koide et al.

The Office rejected independent claim 1 and dependent claims **3, 4, 8, 12** under 35 U.S.C. §102(a) as being unpatentable over Koide et al. (US2001/0048112)(US 6040588). Loss of right to patent under §102(a) requires that the invention be known or used by others in this country or be patented or described in a printed publication before the invention by the applicant. Koide et al. describes a LED where the uppermost barrier layer of a quantum well structure is grown to an additional thickness to allow for some lose of that layer when the next layer of group III-nitride is grown at a higher temperature where some of the $In_yGa_{1-y}N$ will be lost from the structure. It does not teach the suppression of cracking by the growth of stress-relieving interlayers to enable a high-reflectivity DBR as in our invention. It does not, therefore, show that the invention was known by others before our invention as claimed in independent claim 1 and dependent claims 3,4, 8, and 12.

V. DISCUSSION - 35 U.S.C. §102(a) Khare et al.

The Office rejected independent claim **1** and dependent claims **3, 4, and 8** under 35 U.S.C. §102(a) as being unpatentable over Khare et al. (US6576932). Loss of right to patent under §102(a) requires that the invention be known or used by others in this country or be patented or described in a printed publication before the invention by the applicant. Khare et al. describes an LED structure in which the base layer is grown on a substrate which has been intentionally misaligned from a main crystal plane. It does not teach the suppression of cracking by the inclusion of stress-relieving interlayers to enable a high-reflectivity DBR as in our invention. It does not, therefore, show that the invention was known by others before our invention as claimed in independent claim 1 and dependent claims 3,4, and 8.

VI. DISCUSSION - 35 U.S.C. §103(a) Nunoue et al.

The Office rejected independent claims **13 and 14** and dependent claims **5-7, and 10** under 35 U.S.C. §103(a) as being unpatentable over Nunoue et al. (US 20020036295)(2000-289396).

PAGE 12/27 * RCVD AT 2/6/2004 10:55:25 AM [Eastern Standard Time] * SVR:USPTO-EFXRF-1/1 * DNIS:8729306 * CSID: * DURATION (mm-ss):08-44

In order to establish a *prima facie* case of obviousness, there must be some teaching, motivation, or suggestion, supported by objective evidence of record, to modify the reference and the reference must teach or suggest all the claim limitations. Nunoue et al. teaches a DBR comprising a plurality of semiconductor layers made of nitride semiconductor and a plurality of organic layers alternately laminated. It does not teach, motivate, or suggest the growth of a stress-reducing interlayer within the semiconductor heterostructure. Since a prima facie case of obviousness has not successfully been made, the rejection under 35 U.S.C. § 103(a) has been overcome. Accordingly, claims 5-7, 10, 13, and 14 are now in condition for allowance.

Conclusion

Applicants have responded to each and every objection and rejection, and urge that Claims **1-14** as presented are now in condition for allowance. Applicants request expeditious processing to issuance.

Respectfully submitted,

Carol I. Ashby
Agent for Applicant
Registration No. P54,969
Sandia National Laboratories
Patent and Licensing Center, Org. 11500
P.O Box 5800, MS 0161
Albuquerque, NM 87185-0161
Telephone (505) 844-2303
Fax No. (505) 844-1418

PAGE 13/27 * RCVD AT 2/6/2004 10:55:25 AM [Eastern Standard Time] * SVR:USPTO-EFXRF-1/1 * DNIS:8729306 * CSID: * DURATION (mm-ss):08-44

Feb-06-04 09:01am From- T-952 P.018/027 F-134

IEEE JOURNAL OF QUANTUM ELECTRONICS, VOL. QE-10, NO. 4, APRIL 1974

Principles of Distributed Feedback and Distributed Bragg-Reflector Lasers

SHYH WANG, MEMBER, IEEE

Abstract—Wave propagation in periodic waveguides is analyzed by decomposing the eigen Bloch waves into traveling-wave components. It is shown that the principal components consist of a primary forward wave, a primary backward wave, and their Bragg-scattered secondary waves. One important parameter is the coupling constant s due to Bragg scattering, which relates the secondary wave to the respective primary wave. Laser threshold condition is then obtained by applying the continuity of tangential E and H at the two boundaries. The results thus obtained are general and applicable to thin-film lasers with various waveguide structures.

The laser threshold condition of thin-film Bragg lasers is expressed in terms of two effective reflection coefficients for easy comparison with conventional lasers. For appreciable reflection, a significant change either in the propagation constant or in the coupling constant is required. Two basic types of thin-film Bragg lasers are distributed-feedback (DFB) lasers in which Bragg scattering is confined to the active medium and distributed-Bragg-reflector (DBR) lasers in which Bragg scattering is limited to regions beyond the active medium. The threshold gain, frequency control, and mode selectivity for both types are analyzed and the analyses are applied to GaAs and Nd lasers. It is shown that DBR lasers should have a lower threshold gain and a better mode selectivity than DFB lasers. For distributed-feedback effect to play a significant role in thin-film Bragg lasers, the product κL_{int} must be greater than unity where κ is the distributed-feedback coefficient and L_{int} is the interaction length. Advantages for having periodic structures outside the active medium so as to relax constraints on κ and L_{int} are also discussed.

I. Introduction

THE WORK of Kogelnik and co-workers [1], [2] on distributed feedback (DFB) lasers has stimulated a great deal of interest in the use of Bragg scattering to provide the necessary feedback in thin-film lasers. Since the initial work of Kogelnik *et al.*, a number of DFB laser experiments have been reported [3]–[9] by different groups using different laser materials in various experimental configurations. On the theoretical side, several papers discussing the threshold condition and other related aspects of DFB lasers have been published [10]–[13] and new periodic waveguide structures suitable for solid-state and semiconductor lasers have been proposed [11]. In the experimental work reported thus far, only DFB dye lasers have been extensively studied and have shown that their threshold condition can be easily satisfied. Experimental data on DFB GaAs lasers, on the other hand, have indicated that the threshold gain needed in DFB lasers far exceeds that needed in injection lasers. Furthermore, successful operation has been achieved only at 77 K under pulsed conditions. It is the purpose of the present paper to examine the principles underlying the operation of DFB lasers and to consider various types of waveguide structures for optimization of DFB laser performance.

The theoretical analyses reported in the literature are all based on the coupled-wave equation from which the spatial dependence of the complex amplitudes of the field is found. The present analysis departs from the previous analyses at the outset in the approach to the problem. It starts out from finding the eigenmodes of wave propagation in a periodic structure. The eigenmodes that are of the Bloch-wave type are then decomposed into traveling-wave components so that the physical processes going on in a periodic waveguide can be clearly seen and approximation methods can be used in subsequent analysis. Next the threshold condition is obtained for DFB lasers by applying the proper boundary conditions (tangential E and H being continuous) to different laser structures. The results thus obtained are general and can be directly applied to any given DFB laser in terms of physical parameters which are related to the physical properties of the laser structure. Our final aim is to consider the potentials of DFB lasers for use in integrated optics. If thin-film DFB lasers are to be used in future optical communication systems, they must be able to compete in performance with conventional lasers, especially semiconductor injection lasers. In our final analysis, the performance of DFB lasers of various types is discussed with particular emphasis on the threshold gain, frequency control, and mode selectivity of these devices.

II. Wave Propagation in Periodic Waveguides

In this section, we review the essential features of wave propagation in a periodic waveguide. Consider an optical waveguide (Fig. 1) made of a thin film sandwiched between a substrate and a top dielectric layer (superstrate). For a proper mode of wave propagation, the transverse wavenumber k_x must satisfy the following characteristic equation:

$$2k_xW - 2\phi_s - 2\phi_t(d) = 2\pi m, \tag{1}$$

where ϕ_s and ϕ_t are, respectively, the phase shifts at the film-substrate and film-top layer boundary, W is the film thickness, and m is an integer representing the transverse mode number. If the thickness d of the top layer is comparable to, or smaller than, the penetration depth of the evanescent wave in the top layer, then the phase shift ϕ_t is dependent on d. Thus, by varying either the thickness d of

Manuscript received September 25, 1973; revised December 18, 1973. This work was supported in part by the Air Force Office of Scientific Research under Grant AFOSR-71-2114 and in part by the Office of Naval Research under Contract N00014-69-A-0220-1063.

The author is with the Department of Electrical Engineering and Computer Sciences and the Electronics Research Laboratory, University of California, Berkeley, Calif. 94720.

PAGE 18/27 * RCVD AT 2/6/2004 10:55:25 AM [Eastern Standard Time] * SVR:USPTO-EFXRF-1/1 * DNIS:8729306 * CSID: * DURATION (mm-ss):08-44

Feb-06-04 09:01am From- T-952 P.019/027 F-134

Effect of layer thickness variations in a distributed-Bragg-reflector mirror on the phase of the reflected light

Jean-Pierre Weber and Shyh Wang

Department of Electrical Engineering and Computer Science, University of California, Berkeley, Berkeley, California 94720

Received December 26, 1989; accepted March 5, 1990

We present an analytical derivation of the phase change of the reflection coefficient of a distributed-Bragg-reflector mirror when the thickness of a layer in the mirror changes. These phase changes are additive, as has been verified by an exact numerical calculation using transmission matrices. Such a phase change will affect the lasing wavelength of vertical-cavity surface-emitting lasers and the center wavelength of various integrated Bragg devices.

Distributed-Bragg-reflector (DBR) mirrors are now being used in a variety of devices, such as vertical-cavity surface-emitting lasers[1-3] and electroabsorptive reflection modulators.[4] If these devices are to be mass produced with reproducible characteristics, it is important to know what the tolerances are for parameters such as the layer thicknesses. In this Letter we look at one aspect of this problem: the change of the phase of the reflected light when there is a small change in thickness of some layers of the DBR mirror. Using eigenmode theory for periodic structures,[5] we derive an analytic expression that is in good agreement with an exact numerical calculation using transmission matrices. An application of this result to the variation of the lasing wavelength of a vertical-cavity surface-emitting DBR laser has been described elsewhere.[6]

First, let us look at a quick summary of some results of eigenmode theory that we will need in this Letter (their derivation can be found in Ref. 5). If we have a one-dimensional even periodic structure of period Λ, the solution of the wave equation around the Bragg wavelength is of the Floquet–Bloch type and can be written as

$$\begin{aligned} E(z,\lambda) &= A_0[1 + s(\lambda)\exp(j2K_B z)]\exp(\Gamma z) \\ &\quad + B_0[1 + s(\lambda)\exp(-j2K_B z)]\exp(-\Gamma z) \\ &= A_0(1 + s_f)\exp(\Gamma z) + B_0(1 + s_b)\exp(-\Gamma z), \end{aligned} \tag{1}$$

where $K_B = p\pi/\Lambda$ (p is the order of the Bragg reflection) and A_0 and B_0 are the amplitudes of a forward and backward propagating modes, respectively. Note that the origin ($z = 0$) must be a point of even symmetry. The other coefficients are defined by

$$\delta = K_B - \bar{\beta}(\lambda), \tag{2a}$$

$$(G + j\delta_{\text{eff}})^2 = (g + j\delta)^2 + \kappa^2, \tag{2b}$$

$$\Gamma = G + j\delta_{\text{eff}} - jK_B, \tag{2c}$$

$$s = \frac{j\kappa}{G + g + j(\delta + \delta_{\text{eff}})}, \tag{2d}$$

where g and $\bar{\beta}(\lambda)$ are the average amplitude gain and propagation constant, respectively, in the periodic structure and κ is the coupling constant [$=\beta_p$, the coefficient of $\exp(jp2\pi/\Delta z)$ in the Fourier expansion of $\beta(z)$]. Equation (2b) is the dispersion relation of the periodic structure. If only the index of refraction is periodic, κ is real and, in the stop band ($|\delta| < \kappa$), $G < 0$ if $g \le 0$ and $G > 0$ if $g > 0$. From the continuity of the tangential electric and magnetic fields, we can compute the reflection and the transmission coefficients between a uniform and a periodic region.

Figure 1 shows the model that we use: the DBR mirror is considered to be semi-infinite and lossless. We want to find the change of the phase of the reflection coefficient R_T when we insert a small section of thickness t and propagation constant β_t at a distance L from the uniform region. We are concerned here only with the high-reflectivity region (i.e., the stop band). If we neglect the differences in propagation constants of the periodic region with the uniform region and with the inserted section, we can write the reflection and transmission coefficients of Fig. 1 as

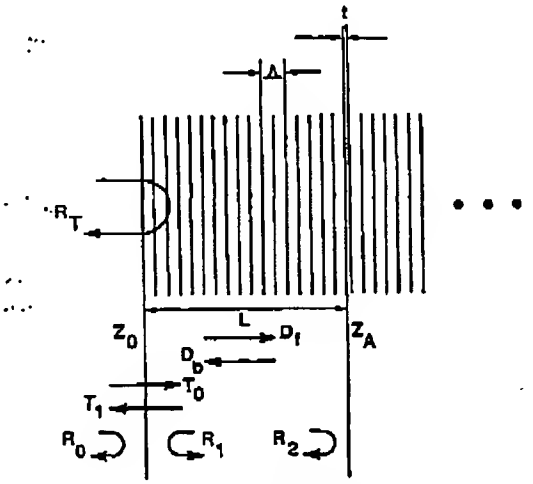

Fig. 1. Model of the DBR mirror.

0146-9592/90/100526-03$2.00/0 © 1990 Optical Society of America

PAGE 19/27 * RCVD AT 2/6/2004 10:55:25 AM [Eastern Standard Time] * SVR:USPTO-EFXRF-1/1 * DNIS:8729306 * CSID: * DURATION (mm-ss):08-44

$$R_0 = s_{f0}, \qquad T_0 = [1 + s_{f0}],$$

$$R_1 = s_{b0}\left[\frac{1 + s_{f0}}{1 + s_{b0}}\right], \qquad T_1 = \frac{1 - s_{f0}s_{b0}}{[1 + s_{b0}]},$$

$$R_2 = \frac{(P_A^2 - 1)s_{fA}}{1 - P_A^2 s_{fA}s_{bA}}\left[\frac{1 + s_{bA}}{1 + s_{fA}}\right], \qquad P_A = \exp(-j\beta_t t),$$

$$D_f = \exp(\Gamma L)\left[\frac{1 + s_{fA}}{1 + s_{f0}}\right], \qquad D_b = \exp(\Gamma L)\left[\frac{1 + s_{b0}}{1 + s_{bA}}\right], \tag{3}$$

where R_2 is obtained by summing multiple reflections and D_f and D_b are the forward and backward propagation factors, respectively. The terms enclosed by the square brackets can be omitted because they will cancel out. By summing the series of multiple reflections, the total reflection coefficient R_T is obtained:

$$R_T = r\exp(i\phi) = R_0 + \frac{R_2 T_0 T_1 D_f D_b}{1 - R_1 R_2 D_f D_b}. \tag{4}$$

If we have no added thickness ($t = 0$), $R_2 = 0$ and the total reflection coefficient $R_T^{(0)} = R_0$. If we have an added thickness t, we get $R_T^{(t)}$. The phase change $\Delta\phi$ is then given by

$$\Delta\phi = \phi^{(t)} - \phi^{(0)} = \arg\left[\frac{R_T^{(t)}}{R_T^{(0)}}\right]. \tag{5}$$

With Eqs. (1)–(4), we get

$$\frac{R_T^{(t)}}{R_T^{(0)}} = \frac{1 - P_A^2 s^2 + (P_A^2 - 1)\exp(2GL)}{1 - P_A^2 s^2 + s^2(P_A^2 - 1)\exp(2GL)}, \tag{6}$$

where we used the fact that $L = z_A - z_0$ and that $\delta_{\text{eff}} = 0$ in the stop band if $g = 0$ (the lossless case). In the lossless case, we can also define

$$s = \exp(-j\psi)$$

with

$$\cos(\psi) = \delta/\kappa$$

and

$$\sin(\psi) = [1 - (\delta/\kappa)^2]^{1/2}. \tag{7}$$

With these results, we can write Eq. (5) as

$$\Delta\phi = \arctan\left\{\frac{\sin[2(\psi + \beta_t t)] - \exp(2GL)\sin(2\beta_t t)}{1 - \cos[2(\psi + \beta_t t)] + \exp(2GL)[\cos(2\beta_t) - 1]}\right\}$$

$$- \arctan\left(\frac{\sin[2(\psi + \beta_t t) + \exp(2GL)\{\sin(2\psi) - \sin[2(\psi + \beta_t t)]\}}{1 - \cos[2(\psi + \beta_t t)] + \exp(2GL)\{\cos[2(\psi + \beta_t t)] - \cos(2\psi)\}}\right). \tag{8}$$

This is an exact result within the eigenmode theory approximation.

However, this result is too bulky to use easily. The quantity $\beta_t t$ is very small (of the order of 0.02) because, for most problems of interest, the added thickness is of the order of a few monolayers. So, if we expand Eq. (8) to first order in $\beta_t t$ and use the trigonometric identity $\tan(A - B) = [\tan(A) - \tan(B)]/[1 + \tan(A)\tan(B)]$, we finally get

$$\Delta\phi = \arctan[-2\beta_t t\exp(2GL)] \approx -2\beta_t t\exp(2GL). \tag{9}$$

Let us note that this result is now independent of ψ and depends only on G ($= -\sqrt{\kappa^2 - \delta^2}$), L, and the added optical length.

The same result can also be obtained in a more intuitive way. Let us call ϕ the phase of the reflected wave when there is no added thickness [$R_T^{(0)} \approx \exp(j\phi)$]. If there is an added thickness, the fraction of the wave that penetrates the mirror further than L will contribute with a phase ($\phi - 2\beta_t t$). The fraction that reaches L is $\exp(GL)$, but then only a fraction $\exp(GL)$ of that comes back to the front facet, so that we can write

$$R_T^{(t)} \approx [1 - \exp(2GL)]\exp(j\phi) + \exp(2GL)\exp[j(\phi - 2\beta_t t)]$$

$$\approx [1 - j2\beta_t t\exp(2GL)]\exp(j\phi), \tag{10}$$

again to first order in $\beta_t t$. And

$$\Delta\phi = \arg\left[\frac{R_T^{(t)}}{R_T^{(0)}}\right] \approx \arctan[-2\beta_t t\exp(2GL)], \tag{11}$$

which is the same result as relation (9).

We now consider the example of a DBR mirror as it could be used for a vertical-cavity surface-emitting laser (but the theory applies to any DBR mirror made of any material). Figure 2 shows a comparison of the result from relation (9) with exact calculations by using transmission matrices (we used a method similar to that in Ref. 7). It is a first-order Bragg mirror and consists of 25 pairs (numbered from 1 to 25, starting from the left). A GaAs region is at the right of the figure, and the surface with air is on the left. Each pair has a 61.63-nm layer of $Al_{0.05}Ga_{0.95}As$ and a 66.75-nm layer of $Al_{0.45}Ga_{0.55}As$, with the leftmost layer in Fig. 2 being $Al_{0.05}Ga_{0.95}As$. We took the refractive indices to be $n(\text{GaAs}) = 3.614$, $n(x = 0.05) = 3.569$, and $n(x = 0.45) = 3.294$ from a model that we developed based on the formulas in Ref. 8. This gives a center wavelength of 879.78 nm, and we assumed a loss of 3 cm^{-1} for the mirror. The example of Fig. 2 was done for a lasing wavelength of 876.51 nm. The horizontal axis is labeled in pairs, with each pair being 128.38 nm. Vertically, we have the phase change due to the addition of a thickness $t = 0.56$ nm (one lattice period) at that position (i.e., in one of the two layers of that pair). We look at the mirror from the GaAs region, i.e., from the right. The exact result exhibits steps because it does not matter where we add the thickness t within a layer. The coupling coefficient κ is 6239 cm^{-1} and $\delta = -91.26$ cm^{-1}, which gives $G = -6238.3$ cm^{-1}. If the thickness is added to the $Al_{0.05}Ga_{0.95}As$ layer, we get $\beta_t t$

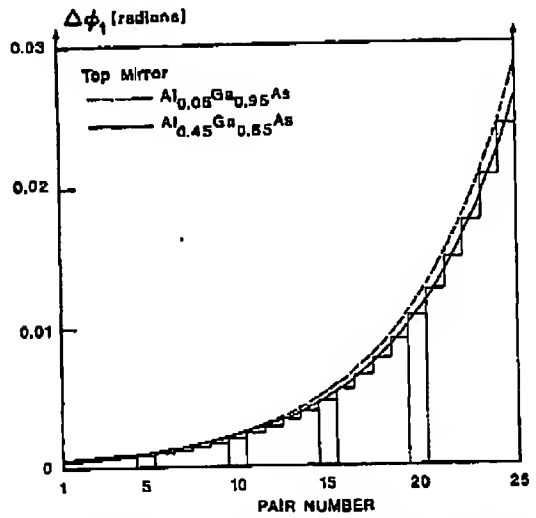

Fig. 2. Absolute change of the phase of the reflection coefficient of the mirror due to one more monolayer as a function of position in the mirror. The steps are exact calculations, and the curves are analytical approximations.

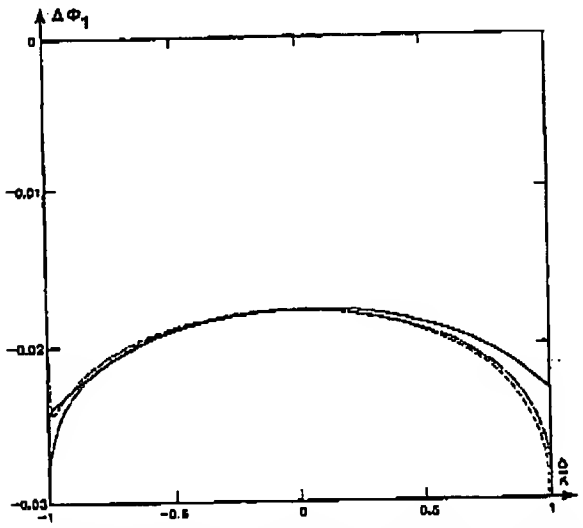

Fig. 3. Phase change as a function of δ/κ for one more monolayer in the $Al_{0.05}Ga_{0.95}As$ layer of pair 23. The solid curve is the exact numerical calculation, the dashed curve is from Eq. (8), and the dashed–dotted curve is the approximation from relation (9).

$= 0.0143$; if the thickness is added to the $Al_{0.45}Ga_{0.55}As$ layer, we get $\beta_1 t = 0.0132$. We see that although the real mirror is finite and not lossless, we have a good agreement between the numerical result and the approximation of relation (9).

These results are for the addition of one thickness t. If we remove a thickness t, we just have to change the sign of t in the formulas, which is equivalent to subtracting the correct optical path length. A comparison with numerical results shows that this procedure is correct. Note that variations in the Al content of the layers will change the index of refraction and thus the optical path length. This will have the same effect as adding or subtracting a certain thickness of material. If we have several thicknesses added or subtracted in a mirror, we can find the total phase change by adding the contribution of each thickness computed with relation (9). We checked this by exactly computing the phase changes due to each thickness separately and comparing the total with the exact calculation with all the thicknesses. The relative error for three thicknesses was less than 0.1%.

Figure 3 shows the phase change for adding a thickness t to the $Al_{0.05}Ga_{0.95}As$ layer of pair 23 as a function of wavelength in the stop band. We can compare the exact numerical result, the exact result [Eq. (8)] of eigenmode theory, and the approximation [relation (9)]. The results from relations (8) and (9) agree well over the range $|\delta| < 0.9\kappa$, and they agree with the exact result with a relative error of less than 10% over the same range.

In conclusion, we have derived an analytical formula for the change of the phase of the reflectivity of a DBR mirror due to thickness and/or composition variations. This formula gives a good approximation of the exact result obtained with a transmission matrices technique. If there are several thickness changes, the phase changes are additive, up to a high degree of precision.

This research was supported by the Air Force Rome Air Development Center and Lockeed Missiles and Space Company. The authors thank Kevin Malloy for his encouragement and suggestions during this research.

The authors are also with the Electronics Research Laboratory, University of California, Berkeley.

References

1. F. Koyama, S. Kinoshita, and K. Iga, Appl. Phys. Lett. 55, 221 (1989).
2. D. Botez, L. M. Zinkiewicz, T. J. Roth, L. J. Mawst, and G. Peterson, IEEE Photon. Tech. Lett. 1, 205 (1989).
3. P. L. Gourley, T. M. Brennan, B. E. Hammons, S. W. Corzine, R. S. Geels, R. H. Yan, J. W. Scott, and L. A. Coldren, Appl. Phys. Lett. 54, 1209 (1989).
4. R. H. Yan, R. J. Simes, and L. A. Coldren, Appl. Phys. Lett. 55, 1946 (1989).
5. S. Wang, in *Semiconductors and Semimetals*, W. T. Tsang, ed. (Academic, New York, 1985), Vol. 22, Part E, pp. 52–64.
6. J.-P. Weber, K. Malloy, and S. Wang, IEEE Photon. Tech. Lett. 2, 162 (1990).
7. G. Björk and O. Nilsson, IEEE J. Lightwave Technol. 5, 140 (1987).
8. S. Adachi, J. Appl. Phys. 58, R1 (1985).

Distributed Bragg Reflectors for Vertical-Cavity Surface-Emitting Lasers

W.G. Breiland, A.A. Allerman, J.F. Klem, and K.E. Waldrip

Abstract

Distributed Bragg reflectors (DBRs) not only serve as high-reflectance mirrors to define the laser cavity of a vertical-cavity surface-emitting laser (VCSEL), but they also must conduct electricity, confine currents, and provide a single-crystal template for the gain region of the laser. Basic optical and electrical properties of DBRs are presented in this article. Three examples of DBR structures used in VCSEL applications from the ultraviolet to the infrared are given to illustrate the complexity and range of materials science issues that are encountered in DBR growth. Fabrication issues are also discussed.

Keywords: chemical vapor deposition (CVD), compound semiconductors, optoelectronic materials, vertical-cavity surface-emitting lasers (VCSELs).

Introduction

The distributed Bragg reflector (DBR) is used primarily in vertical-cavity surface-emitting laser (VCSEL) applications as a mirror for confining the electric field within the optical cavity and gain region. It thus serves the same function as a metallic or dielectric mirror in a conventional laser. Very high reflectivity is required because the single-pass gain can be less than 1% in the short cavities used for VCSELs.

If the reflectance property were the only function served by the DBR, fabrication would be straightforward. However, the DBRs in a VCSEL must also satisfy several additional constraints. The DBR must often carry current to the gain region, requiring that it be a low-resistance electrical conductor. The current and optical fields must be laterally confined to optimize device performance. Additionally, VCSELs exhibit complex temperature effects, and the thermal conductivity of the DBR can be a critical property. To preserve single-crystal band-state properties that allow the gain region to function, the bottom DBR of a VCSEL must be grown epitaxially.

These electronic and materials constraints pose challenges to the device designer and grower. It is common for a DBR structure to contain over 100 individual layers with complex, graded composition and doping profiles. Such complexity results in a VCSEL whose total thickness is mostly taken up by two DBRs, with only a small fraction of the device devoted to the optical cavity and gain region.

This article describes the use of DBRs in VCSEL applications. Basic optical and electronic properties are reviewed. Fabrication issues arising from optical and electronic constraints are discussed. Finally, applications of three representative VCSEL devices are described to illustrate the complexity and range of materials science issues that are encountered in DBR growth.

Distributed Bragg Reflectors: Basics

Optical Properties of a Distributed Bragg Reflector

The distributed Bragg reflector nomenclature traces back to the use of external periodic grating structures as wavelength-selective cavity mirrors in edge-emitting lasers. However, for VCSEL applications, it is more convenient to view a DBR structure as a multilayer thin-film mirror, much like a conventional dielectric mirror.

The basic optical properties of a DBR may be derived from the normal-incidence Fresnel reflection coefficient r for an interface between two media with refractive-index values n_1 and n_2:

$$r = \frac{n_1 - n_2}{n_1 + n_2} \quad (1)$$

The observable interface reflectance R from such an interface is the square of the reflection coefficient, $R = |r|^2$. If $n_1 < n_2$, r is negative, implying that the electric field undergoes a 180° phase shift upon reflection. No such phase shift occurs if $n_1 > n_2$. These different phase-shift behaviors are exploited in a DBR.

A simple DBR structure is shown in Figure 1a. The mirror is designed to have a maximum reflectance at a specified wavelength, λ_0, the "design" wavelength. Two different transparent materials are used, one with a higher refractive index, n_H, and one with a lower refractive index, n_L. Each layer in the DBR structure is made to be exactly one-quarter of a wavelength thick, $d_H = \lambda_0/4n_H$ and $d_L = \lambda_0/4n_L$, where the film thickness d is determined by the wavelength that is present *inside* each material layer. In other words, the quarter-wave thickness refers to the optical, rather than the physical, path length of light through the film.

The repeated layers shown in Figure 1a lead to the term "quarter-wave stack" to describe a DBR. It is also referred to as a bilayer stack, or binary stack, because it consists of repeated low-index and high-index (LH) quarter-wave bilayers. Each bilayer pair of layers is also called a "period" of the DBR stack, leading to the term "m-period stack." For highest reflectivity, the DBR is terminated at each end with a high-index layer, as shown in Figure 1a. The extra H layer added to the m periods is called an m.5-period stack.

The reflectance from the stack of layers is determined by the combined amplitudes of all electric fields reflecting from all

PAGE 22/27 * RCVD AT 2/6/2004 10:55:25 AM [Eastern Standard Time] * SVR:USPTO-EFXRF-1/1 * DNIS:8729306 * CSID: * DURATION (mm-ss):08-44

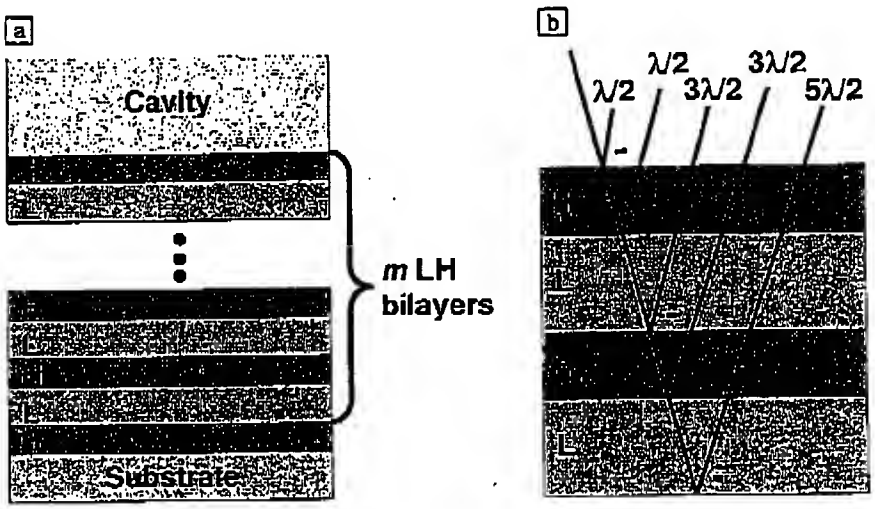

Figure 1. (a) Distributed Bragg reflector (DBR) structure using a high-refractive-index quarter-wave layer on the substrate followed by m low-index/high-index (LH) quarter-wave bilayers. (b) Relative phases at the DBR surface of light rays reflected from each interface within the DBR structure. The minus sign indicates the 180° phase shift that occurs upon reflection from a low- to high-index surface. A round-trip pass through each quarter-wave layer results in a half-wave phase shift. Every reflected ray returns to the DBR surface shifted by exactly 180° in phase. All reflected electric fields thus add constructively to give a high net reflectance for the DBR, even if individual interface reflectances are small.

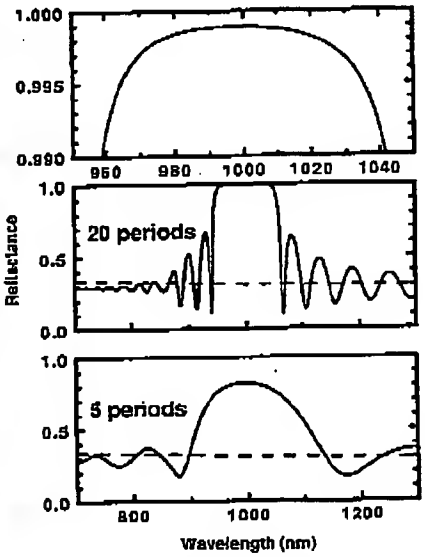

Figure 2. Reflectance spectrum in air of a 1000-nm GaAs/AlAs DBR for 20 periods and 5 periods (lower two plots). Dashed lines show the reflectance from a bare GaAs substrate. Top plot shows the high-reflectance region of the 20-period mirror near the design wavelength.

interfaces in the DBR structure. Figure 1b illustrates how the combination of phase shifts and round-trip optical path lengths conspire to bring each reflected component exactly in phase (within a multiple of one wavelength) with all other components at the top surface of the DBR. If enough layers are used, very high reflectance can be achieved, even with materials whose single-interface reflectance (r) values are quite low. When $n_H \cong n_L$, then $|r| << 1$ and the system is said to have low contrast. Most compound-semiconductor DBR stacks have low-contrast interfaces.

Figure 2 shows theoretical reflectance spectra in air of a DBR with a design wavelength of 1000 nm during various stages of growth. High-index layers use GaAs ($n = 3.509$) and are 71.25 nm thick. Low-index layers use AlAs ($n = 2.949$) and are 84.77 nm thick. As more quarter-wave layers are added to the structure, the reflectance spectrum acquires more oscillatory features, and a narrow, flat-topped high-reflectance region grows around the 1000-nm design wavelength. It takes 14 layers to achieve a peak reflectance of 99%. A peak reflectance of over 99.9% requires 21 layers.

The reflectance behavior shown in Figure 2 may be quantified with multilayer thin-film optical models.[1] Given that one knows the refractive indices of the substrate, n_s, the cavity region, n_c (the "cavity" could also be air, $n_c = 1$), and the high- and low-index materials, n_H and n_L, the reflectance coefficient inside the cavity region at the design wavelength of the m-period bilayer structure shown in Figure 1 is:

$$r(\lambda_0) = -\frac{1-\alpha}{1+\alpha}, \tag{2}$$

$$\alpha = \frac{n_s n_c}{n_H^2}\left(\frac{n_L}{n_H}\right)^{2m}, \tag{3}$$

and

$$R(\lambda_0) = |r(\lambda_0)|^2. \tag{4}$$

The reflectance can be made as close to 100% as desired by making α sufficiently small.

Small α values are achieved with high-contrast bilayers, $n_H >> n_L$, or by using many such bilayers in the stack, $m \to \infty$. Acceptable DBR materials for high-contrast bilayers are difficult to find because most lattice-matched compound semiconductors have similar refractive-index values. Therefore, the only alternative is to use many bilayers in the DBR stack. Unfortunately, there is a diminishing-returns effect—the absolute increase in reflectance is less with each additional period.

The expression $m \to \infty$ may be solved for m to determine the number of bilayers that will be needed to achieve a desired R for a given materials system:

$$m = 0.5 \ln\left[\frac{n_H^2(1-\sqrt{R})}{n_s n_c(1+\sqrt{R})}\right] / \ln(n_L/n_H). \tag{5}$$

In practice, more layers than predicted by Equation 5 may be needed, due to fabrication errors in the layer thickness and scattering from rough interfaces. Effects of fabrication errors have been discussed by Weber et al.[2]

Another quantity of interest is the spectral width of the reflectance region. In units of normalized wave number, $\bar{\nu} \equiv \lambda_0/\lambda$, the half-maximum reflectance values are observed at $1 \pm \Delta\bar{\nu}$, with

$$\Delta\bar{\nu} = \frac{2}{\pi}\sin^{-1}\left(\frac{n_H - n_L}{n_H + n_L}\right), \tag{6}$$

where $\Delta\bar{\nu}$ is the spectral width. High DBR reflectance and broad spectral range are both favored by high-contrast bilayers. Note that the formulas for m and $\Delta\bar{\nu}$ are not explicitly dependent on the design wavelength.

VCSEL performance is maximized when the three wavelengths associated with maxi-

PAGE 23/27 * RCVD AT 2/6/2004 10:55:25 AM [Eastern Standard Time] * SVR:USPTO-EFXRF-1/1 * DNIS:8729306 * CSID: * DURATION (mm-ss):08-44

mum gain, cavity resonance, and maximum DBR reflectance have identical values. The top graph in Figure 2 shows that the maximum in reflectance has significant curvature near the design wavelength. Losses from less-than-maximum reflectance will pull the lasing wavelength toward the DBR maximum. Because the refractive-index-dispersion spectra of all semiconductors are temperature-dependent, the DBR maximum and cavity resonance will shift with temperature. The gain region is typically sensitive to temperature also. Some continuous-wave VCSEL designs use DBR structures to optimize VCSEL performance at a given operating temperature.

For optimal VCSEL design, it is not sufficient to treat the mirrors, cavity, and gain region as independent design elements. Modeling of the standing waves that are generated in the entire structure becomes essential. The results of such a model are shown in Figure 3. Note that the electric field extends deep within each of the DBRs, graphically illustrating the mirror, cavity, and gain interdependence.

Electrical Properties of a DBR

Unless the VCSEL is pumped externally by means of laser or electron-beam sources, electrical injection must be supplied to the gain region in order to cause laser action. The configuration of a VCSEL typically requires that current flow through at least part of one DBR. Unfortunately, the simple LH quarter-wave bilayers introduced in the previous section are not ideal electrical conductors. The different bandgaps at layer interfaces present barriers to electrical conduction and cause scattering and high electrical resistance. The high resistance reduces efficiency and leads to heating, which degrades laser performance.

A compromise between optical and electrical properties can be achieved. The composition of the bilayers may be smoothly modulated.[3] Gradual changes in composition yield small changes in bandgap and less carrier scattering. The modulation can be adjusted such that the optical phase-shift properties illustrated in Figure 1 are still satisfied, although more layers are needed to achieve the same reflectance as a simple stack of bilayers. Doping may also be modulated to optimize resistivity.[3]

DBRs may be used to confine carriers to small lateral dimensions in the vicinity of the cavity and gain region. Selective oxidation of the period next to the optical cavity provides an electrical and waveguiding aperture for more efficient VCSEL operation.[4]

Fabrication Issues in Growing DBRs

VCSEL growth presents one of the most challenging structures faced by practitioners of metalorganic chemical vapor deposition (MOCVD) and molecular-beam epitaxy (MBE). Composition and layer thicknesses must be held to very strict tolerances over hundreds of layers and many micrometers of growth. We have found that such control is significantly enhanced by using *in situ* optical sensors that can measure growth rate and wafer temperature during deposition.

A simple yet powerful optical monitor is to measure the normal-incidence reflectance. Figure 4 shows the spectral history of a 950-nm VCSEL during its entire growth. The buildup of the first DBR, cavity deposition, second mirror, and temperature-dependent refractive-index effects during cooldown are readily seen. Even the formation of the Fabry–Pérot cavity resonance can be observed (thin yellow stripe near the center of the red reflectance maximum in the cooldown region).

In practice, we have found that just a single reflectance wavelength, usually 550 nm, is sufficient to monitor and measure growth. Pre-growth calibration using a virtual interface method[5] for extracting growth rates and optical constants has proven adequate for MOCVD VCSEL fabrication.[6] Real-time control has also been implemented in VCSEL growth using MBE.[7]

Examples of DBR Structures and Growth Techniques

Following are specific examples of DBR structures used for VCSEL applications from UV to IR wavelengths. The DBR structure is given, along with a brief description of the function that each layer serves in the overall structure. Fabrication issues are also addressed where appropriate.

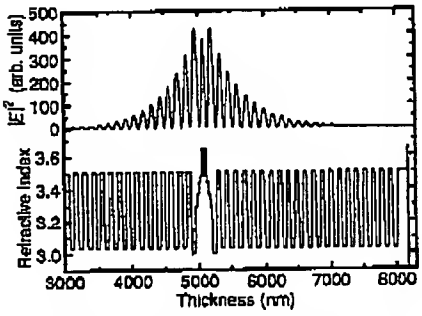

Figure 3. (bottom curve) Refractive-index profile of an 850-nm vertical-cavity surface-emitting laser (VCSEL) structure, omitting 3000 nm of the lower DBR. (top curve) Standing-wave electric-field intensity $|E|^2$ pattern that is established in the VCSEL.

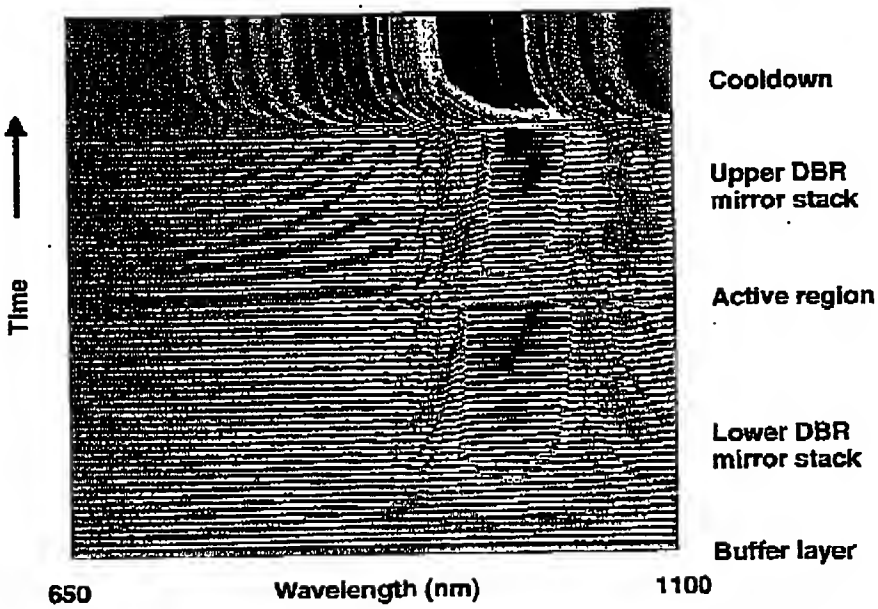

Figure 4. Reflectance spectrum history during the growth of a 950-nm VCSEL using in situ normal-incidence reflectance spectroscopy. Reflectance is plotted in false color, with blue representing low reflectance and red representing high reflectance.

PAGE 24/27 * RCVD AT 2/6/2004 10:55:25 AM [Eastern Standard Time] * SVR:USPTO-EFXRF-1/1 * DNIS:8729306 * CSID: * DURATION (mm-ss):08-44

Example 1: UV DBRs

The III-nitrides are used for short-wavelength visible and ultraviolet VCSEL emission. DBRs with >99% reflectivity in the UV region may be achieved with $Al_xGa_{1-x}N$ (L) and GaN (H). Unfortunately, this combination has low contrast and requires a large number of pairs (50–70) to achieve $R > 99\%$. The resulting thick structure (~4–5 μm) leads to a significant buildup of tensile-stress energy. A 2.54% in-plane biaxial tension exists in AlN when grown epitaxially on GaN by MOCVD at 1050°C, which limits the AlN mole fraction that can be incorporated into the low-index alloy without relaxation. When grown in the (0001) orientation, as is typical, no resolved shear stresses reside on any effective slip systems that would allow relaxation by means of the introduction of interfacial misfit dislocations. This causes the material to fail by means of fracture (i.e., crack formation) prior to plastic deformation. Control of this stress is absolutely essential for successful DBR fabrication.

The use of an *in situ* stress monitor is extremely useful in the design of novel DBR structures employing lattice-mismatched materials and stress-engineering methods.[8] Two parallel laser beams are reflected off the wafer, and the wafer curvature is measured as the change in distance between the two laser spots on a CCD detector. Wafer curvature is proportional to the product of the film stress and the film thickness.

Figure 5 shows three *in situ* stress × thickness curves as a function of film thickness. The top curve in Figure 5 shows stress evolution for 30 pairs of an $Al_{0.20}Ga_{0.80}N$/GaN DBR. Positive slopes indicate tension, while negative slopes indicate compression. The sawtooth-like features are a result of the stresses of individual layers, while the overall stress evolution is dictated by the average composition of the stack. Evidence for relaxation and cracking are seen at 1.35 μm and 2.33 μm. Such cracking leads to unacceptable DBRs.

The middle curve in Figure 5 shows how the stress can be reduced by inserting a thin 135-Å AlN "interlayer" between the 1-μm GaN nucleation layer and the mirror stack, as shown in the inset. No evidence of cracking is seen, presumably because the interlayer relaxes and creates a new lattice template with a smaller in-plane lattice constant for subsequent growth.

Crack-free DBRs with reflectivities of >99% can be achieved through the insertion of multiple interlayers into the stack to "reset" the tensile stress. The bottom curve in Figure 5 shows the stress evolution of a structure similar to the middle curve in the same figure, but with an AlN interlayer inserted after every 20 periods.

Example 2: 850-nm DBRs

A rapidly increasing number of commercial applications for optical interconnects and communications, laser printing, recording, and displays use 850-nm VCSELs. These applications take advantage of the high-quality DBR mirrors that are possible in the AlGaAs material system. This system exhibits relatively high contrast, good thermal conductivity compared with other ternary materials, and the alloy composition is simply controlled by the flux of the Group III atoms. Moreover, the entire range of $Al_xGa_{1-x}As$ alloy compositions are nearly lattice-matched to GaAs substrates. This allows one to design very sophisticated graded structures in composition and doping, in order to optimize VCSEL performance.

A typical lower (bottom of stack) DBR mirror structure for an 850-nm VCSEL consists of a highly reflective (99.9%) mirror formed from 35.5 pairs of compositionally graded $Al_{0.20}GaAs$ and $Al_{0.92}GaAs$. The upper (top of stack) DBR is similar to the lower structure, but the number of pairs are reduced to 19–23 to lower the reflectivity and serve as the output coupler for laser emission. A low-index $Al_{0.98}GaAs$ layer can be inserted just before and immediately following the cavity/gain region. This layer can be partially oxidized after the device structure is grown, forming a current aperture that limits injected current to a very small area in the gain region, again improving device efficiency.[4] Accurate control of composition can be achieved using *in situ* reflectance pregrowth calibration coupled with a simple growth model and an automated growth-recipe generator.[6]

Example 3: 1.3-μm DBRs

VCSELs operating at a wavelength near 1.3 μm may be grown on GaAs substrates and consist largely of the same materials as VCSELs designed for the 780–980-nm region (see Example 2). The high-index DBR material is normally GaAs, and the low-index material is either pure AlAs, or AlGaAs with a high percentage of Al. Optical absorption losses in the DBR materials at 1.3 μm tend to be greater than at shorter wavelengths. These losses are due primarily to free-carrier absorption associated with the doping of the materials required for electrical conductivity. Therefore, special attention must be paid to reducing these losses by optimization of the doping profiles of the DBRs.

The gain region in a 1.3-μm VCSEL often contains a material such as InGaAsN,

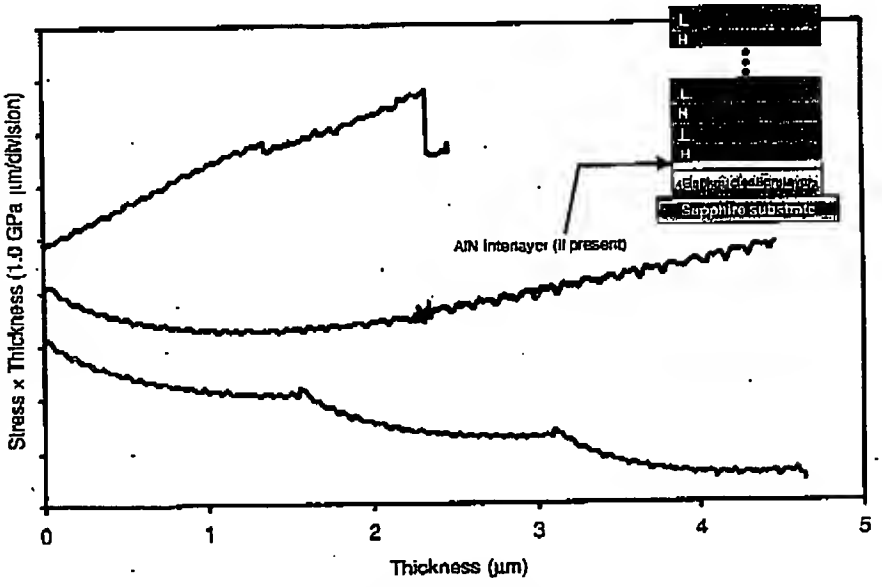

Figure 5. Real-time stress evolution as a function of film thickness for (top curve) 30 pairs of $Al_{0.20}Ga_{0.80}N$/GaN; (middle curve) 60 pairs grown atop an AlN "interlayer" on a GaN template, showing the reduction in stress that can be achieved by inserting a thin 135-Å AlN interlayer between the 1-μm GaN nucleation layer and the mirror stack, as shown in the inset; and (bottom curve) 60 pairs employing three AlN interlayers inserted every 20 periods for stress control. The curves are offset for readability.

PAGE 25/27 * RCVD AT 2/6/2004 10:55:25 AM [Eastern Standard Time] * SVR:USPTO-EFXRF-1/1 * DNIS:8729306 * CSID: * DURATION (mm-ss):08-44

which may dictate the use of MBE rather than MOCVD for growth of the structure. The choice of MBE as the growth technique in turn dictates some aspects of the structure of the DBRs. In particular, continuous compositional grading is more difficult to achieve using MBE than MOCVD. This problem is solved by using very thin (normally 0.3–3 nm) alternating layers of high-index and low-index materials to form a "digital alloy." The digital alloy approximates the properties of a true random alloy of intermediate composition. By changing the relative thicknesses of these layers, any effective composition between those of the high- and low-index materials may be achieved.

Current commercial MBE growth systems offer some advantage over similar MOCVD systems in the form of more flexible computerized control systems. These systems may be used for sophisticated control of the growth of DBR structures and tight control over thicknesses. Using *in situ* normal-incidence reflectance measurements, growth rates of these layers may be determined in real time. Both growth rates and growth times may then be adjusted in a feedback control system to very accurately grow the desired layer thicknesses. In practice, control of the operating wavelength to a level approaching 0.1% has been achieved in MBE-grown 1.3-μm VCSELs using these techniques.

Conclusions

This article has only touched on the subtleties associated with distributed Bragg reflector structures and their growth. Further details may be obtained from the scientific literature. Despite the complexity of DBR structures, robust methods for their fabrication are being developed that are making their way into mass-production facilities. This has led to explosive growth in the number of vertical-cavity surface-emitting lasers produced for a wide variety of commercial applications.

Acknowledgments

Sandia National Laboratories is a multiprogram laboratory operated by Sandia Corporation, a Lockheed Martin Company, for the U.S. Department of Energy under contract No. DE-AC04-94AL85000.

References

1. H.A. MacLeod, *Thin-Film Optical Filters*, 2nd ed. (McGraw-Hill, New York, 1989) p. 164.
2. J. Weber, K. Malloy, and S. Wang, *IEEE Photon. Technol. Lett.* 2 (1990) p. 162.
3. K.L. Lear and R.P. Schneider Jr., *Appl. Phys. Lett.* 68 (1996) p. 605.
4. K.D. Choquette, R.P. Schneider Jr., K.L. Lear, and K.M. Geib, *Electron. Lett.* 30 (1994) p. 2043.
5. W.G. Breiland and K.P. Killeen, *J. Appl. Phys.* 78 (1995) p. 6726.
6. H.Q. Hou, K.D. Choquette, B.E. Hammons, W.G. Breiland, M.H. Crawford, and K.L. Lear, in *Proc. SPIE*, Vol. 3003 (SPIE—The International Society for Optical Engineering, Bellingham, WA, 1997) p. 34.
7. K.D. Choquette, J.F. Klem, A.J. Fischer, O. Blum, A.A. Allerman, I.J. Fritz, S.R. Kurtz, W.G. Breiland, R. Sieg, K.M. Geib, J.W. Scott, and R.L. Naone, *Electron. Lett.* 36 (2000) p. 1388.
8. S. Hearne, E. Chason, J. Han, J.A. Floro, J. Figiel, J. Hunter, H. Amano, and I.S.T. Tsong, *Appl. Phys. Lett.* 74 (1999) p. 356.

2003 Materials Research Society Spring Meeting Announcement & call for papers

2003 MRS SPRING MEETING • APRIL 21-25, SAN FRANCISCO, CA

The 2003 Materials Research Society Spring Meeting will be held April 21–25, 2003, in San Francisco, California, at the San Francisco Marriott and Argent Hotels. The meeting will include 25 symposia that highlight new advances in the understanding, synthesis, and application of materials in diverse fields.

ABSTRACT DEADLINES
OCTOBER 18
for abstracts sent via fax or mail
NOVEMBER 1
for abstracts sent via the MRS Web site
LATE ABSTRACTS WILL NOT BE ACCEPTED.

CONTACT INFORMATION
MRS Materials Research Society
506 Keystone Drive
Warrendale, PA 15086-7573 USA
Tel: 724-779-3003
Fax: 724-779-8313 (general)
724-779-3030 (abstract submittal)
E-mail: info@mrs.org

SCHEDULED SYMPOSIA
ELECTRONIC AND OPTICAL MATERIALS
A: Amorphous and Nanocrystalline Silicon-Based Films—2003
B: Compound Semiconductor Photovoltaics
C: New Applications for Wide-Bandgap Semiconductors
D: CMOS Front-End Materials and Process Technology
E: Materials, Technology, and Reliability for Advanced Interconnects and Low-k Dielectrics
F: Chemical-Mechanical Planarization
G: Integration of Heterogeneous Thin-Film Materials and Devices
H: Flexible Electronics—Materials and Device Technology
I: Optoelectronics of Group-V Based Materials
J: Microphotonics, Nanophotonics, and Photonic Crystals
MOLECULAR MATERIALS AND BIOMATERIALS
K: Molecular-Scale Electronics and Optoelectronics
L: Organic and Polymeric Materials and Devices
M: Nanotube-Based Devices
N: Biomicroelectromechanical Systems (BioMEMS)
O: Materials Inspired by Biology
NANOSTRUCTURED MATERIALS
P: Self-Assembled Nanostructured Materials
Q: Unconventional Approaches to Nanostructures with Applications in Electronics, Photonics, Information Storage, and Sensing
R: Nanomagnetism
S: Nanoscale Thermal Transport—From Fundamentals to Devices
T: Nanostructuring Materials with Energetic Beams
U: Mechanical Properties Derived from Nanostructuring Materials
GENERAL
V: Semiconductor Spintronics II
W: Multiscale Phenomena in Materials—Experiments and Modeling Related to Mechanical Behavior
X: Frontiers of Materials Research
Y: Advanced Optical Processing of Materials
Z: Mechanisms in Electrochemical Deposition and Corrosion

For symposium descriptions, abstract submission instructions, and updated meeting information, visit the MRS Web site:
www.mrs.org/meetings/spring2003/